TECHNICAL PAPER

The effect of hypokyphosis on the biomechanical behavior of the adolescent thoracic spine

Rozilene Maria C. Aroeira[1] · Antônio Eustáquio M. Pertence[2] · Daniel Takanori Kemmoku[3] · Marcelo Greco[1]

Abstract

Deformity in adolescent thoracic spine has high prevalence worldwide. The objective of this work was to study the biomechanical behavior on the thoracic spines of adolescents under asymmetric ligament load in kyphosis and rectified kyphosis. Two finite element models of an adolescent thoracic segment, T5–T10, were generated with every bone component, intervertebral discs, the flavum, intertransverse and supraspinous ligaments. The three-dimensional geometry of the T5-T10 was generated with Autodesk®Maya®, and HyperMesh® version 14.0 was used to generate the finite element models. Asymmetric ligament load of 10 N was applied in the T8–T9, with and without axial load of 400 N in the T5 vertebra. Rectified kyphosis showed the highest rotational displacement of the T8–T9 unit: 0.16° with axial load and asymmetric ligament load, and 0.22° with asymmetric ligament load alone. Kyphosis exhibited rotational displacement of 0.11° and 0.12°, respectively, for the same load conditions. Rectified kyphosis subjected to an asymmetric ligament force showed greater inoperability of the facet joints, and therefore greater vulnerability to vertebral rotation. The results suggest the need for greater attention to the vertebral assessments in the sagittal plane, beginning from the growth spurt period, to adopt preventive therapeutic in vertebral deformities such as adolescent idiopathic scoliosis.

Keywords Kyphosis · Idiopathic scoliosis · Biomechanics · Finite elements · Geometric modeling

1 Introduction

Scoliosis is a three-dimensional deformity of the vertebral column limited to humans, where 80% of cases are adolescent idiopathic scoliosis (AIS), with a prevalence of 2–4% in this age group [40]. A number of theories have been suggested for the cause of AIS. The loading asymmetry on the thorax and spinal structures, generating an asymmetry in bone growth, is defended by some authors

✉ Marcelo Greco
mgreco@dees.ufmg.br

1 Departamento de Engenharia de Estruturas, Escola de Engenharia, Universidade Federal de Minas Gerais, Belo Horizonte, Brazil

2 Departamento de Engenharia Mecânica, Escola de Engenharia, Universidade Federal de Minas Gerais, Belo Horizonte, Brazil

3 Centro de Tecnologia da Informação, Divisão de Tecnologia Tridimensional (DT3D), Campinas, Brazil

[34, 26, 39, 35]. Others suggest that changes in the sagittal profile in the spines of children and adolescents may be considered a risk factor for the onset and progression of AIS [5, 25, 29].

The human spine is the only spine among vertebrates in which the loading sites are directed towards the dorsal portion of the vertebrae [12]. It is a considerably less stable construction in terms of rotational movements when compared to any other found in nature [13]. This phenomenon is a result of the bipedal posture, which significantly changes spinal loading conditions [3]. If dorsally directed, the forces acting on the column can be resolved into an axial component and an anteroposterior shear component [12]. Morphological or postural changes may extend the posterior inclination sites to a larger number of vertebrae, modifying the distribution of the load on these structures. Castelein et al. [3] postulated that AIS has a mechanical basis linked to the action of shear forces directed towards the posterior portion of the vertebrae, compromising its rotational stability. Schlosser et al. [32] suggest that certain sagittal profiles of the spine are more likely to develop rotational deformations, which may lead

to scoliosis. In addition, rotational instability could promote an uneven stimulus for the growth of the vertebral pedicle, worsening the rotation. According to White's [41] theory, an imbalance in growth between the anterior and posterior portions of the vertebra, which may lead to a reduction in kyphosis, could also lead to scoliosis if associated with a small lateral imbalance. The reduction of cervical lordosis and thoracic kyphosis is commonly associated with the phenomenon of AIS [31].

During growth spurts, thoracic kyphosis appears to be slightly reduced, returning to normal afterwards in most cases. Willner and Johnson [42] demonstrated a reduction in the kyphotic arch in the period from 10 to 12 years of age. A significant reduction in kyphosis, called hypokyphosis, occurs early in progressive scoliosis, in contrast to non-progressive scoliosis [29]. Furthermore, radiological, biomechanical, and post-mortem research related to the pathogenesis of idiopathic scoliosis indicates that many normal children have biplanar asymmetry that overlaps during body growth [6]. This uneven distribution of loads can lead to asymmetric growth due to traction on the surrounding soft tissues [16]. Studies by Van Der Plaats et al. [38], and Stokes and Gardner-Morse [36] associated the loading asymmetries in the flavum and intertransverse ligaments with the onset of scoliosis. According to Dickson et al. [6], the association of hypokyphosis and biplanar asymmetry would be one of the triggers for the AIS deformation process.

In the biological field, it is not always possible to do experimental studies. Particularly when adolescent individuals should be tested, the scarcity of anatomical parts and ethical constraints of many studies become impossible. In these cases, in silico studies may be the only available option, although there is little biomechanical and experimental data for calibration of the models that represent the structures of the bones and intervertebral disks in human spine. However, in recent decades, computational studies using the finite element method (FEM) have been successful in biomechanical system analyses, and have made an important contribution to the understanding of the mechanical behavior of the vertebral column [38, 37, 4, 18, 20, 14]. Over time, different geometric models have been used, including everything from simple versions containing beam elements, represented by interconnected cylinders and bars [10], to more comprehensive volumetric models of the spine. The generation of realistic spinal models is of great importance for computational analyses aimed at studying vertebral deformation in adolescents. The most widely used technique that allows 3D geometrical recognition of the human anatomy is based on computed tomography (CT) or magnetic resonance imaging (MRI) data. The advantage of this methodology is that tomographic images can accurately reproduce bone

geometry and generate custom templates. However, the high ionizing radiation index of CT, radio frequencies and electromagnetism of MRI imaging, and the high cost make them unsuitable for acquiring geometric models for non-customized studies [8]. Moreover, these are tests performed with the patient in the supine position, while the upright position is a prerequisite to ensure accurate reproduction of morphological alterations in vertebral deformities [40].

Computational studies on adolescent spines are very rare. Dong et al. [7] worked on a FEM study to assess rupture stress in ligament tissue from the cervical spine of 10-year-old children. No biomechanical studies were found in the literature comparing the adolescent thoracic spine with kyphosis and hypokyphosis. Thus, the objective of this study was to generate two finite element (FE) models for the T5–T10 thoracic segment of an adolescent, showing kyphosis and the absence of kyphosis, and to compare the biomechanical effects in the presence of axial load and asymmetric ligament load.

2 Methods

This study involved two distinct steps: (1) creation of the 3D geometric model of an adolescent's T5–T10 segment, and (2) computational simulation using FEM.

3 3D geometric model

The 3D geometric model was generated using the modeling, simulation and rendering program Autodesk® Maya® 3D (2013). The T5–T10 thoracic segment model was composed of its main elements, such as the vertebrae, the intervertebral disks, and the intertransverse, flavum, and supraspinous ligaments. The vertebrae showed the cortico-cancellous bone, fibrous ring, and nucleus pulposus of the intervertebral disk, and the posterior elements—including the pedicle, lamina, transverse processes, spinal process, and facet joints. The modeling of the vertebrae was initiated using the box modeling process in Autodesk® Maya®, using the sagittal and superior images of vertebra T6, obtained from a human anatomy atlas. The surface modeling of all other vertebrae (T5, T6, T7, T8, T9, and T10) was performed based on the T6 model. The sizing of each vertebra was based on quantitative studies of the 3D anatomy for thoracic vertebrae by Panjabi et al. [28]. Subsequently, the vertebrae were resized for the geometric parameters of the female adolescent spine, according to a study by Meijer et al. [24]. The process of creating and sizing the intervertebral disk followed the same parameters mentioned above. The disk was modeled distinguishing the

structures of the fibrous ring and the nucleus pulposus, where the latter occupied 40% of the center of the disk.

Figure 1 shows the final modeling of the T5–T10 segment, in its separate parts and in RX mode. The main challenge in creating the geometric model lies in modeling the 10 facet joints. Since it is a small anatomic structure, approximately 1 cm high, detail in this region depended on the superior ability of the modeling process. The joint surfaces were considered to exhibit smooth concavity, in addition to apophyseal joint face angulation with a coronal plane, allowing the interline of these apophyses to be contained on a cylindrical surface with an axis at the center of the vertebral body [23], and contact, without overlap, with the mesh generated. Accurate and symmetrical contact is necessary for a successful simulation with FEM. To achieve geometric symmetry, one of the hemiphases was replicated for all the structures of the final model.

Reference values for adult vertebrae dimensions can be found in Panjabi et al. [28]. These dimensions were adapted here for a ten-year woman individual, following Meijer [23] relations. Table 1 presents the considered vertebrae dimensions and the dimensions relations between a ten-year adolescent and an adult individual. Figure 2 presents the vertebra main components.

3.1 Generating the finite element mesh

The geometric model generated using Autodesk® Maya® only consisted of a triangular mesh representing the surface
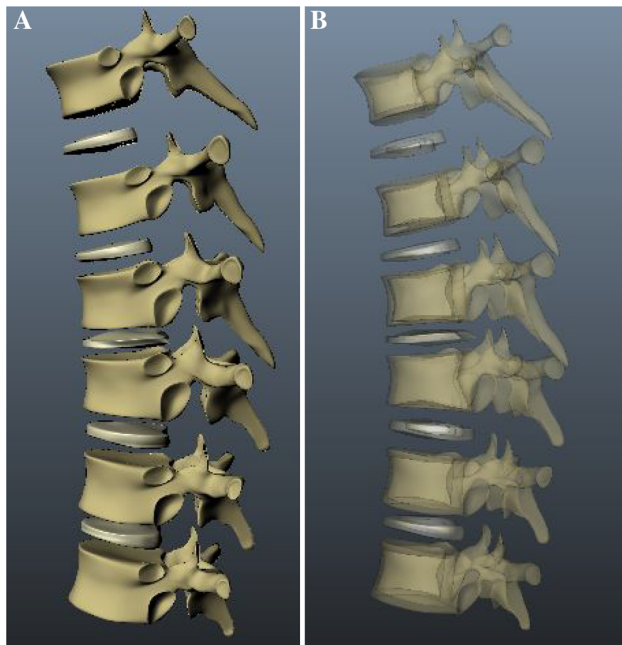
Fig. 1 3D model generated by Maya for individualized visualization (**a**) and in RX mode (**b**)

of the solid. As with other methodologies for obtaining anatomical models, this type of mesh is unsuitable for direct applications in finite element analysis codes. Thus, a 3D model of finite elements was generated by applying a specific mesh generation procedure. This pre-processing was performed using the computer program HyperMesh version 14.0 (Troy, Michigan, USA). For more complex anatomical structures, such as facet joints, fine adjustments were required using MeshMixer (v11.0.544) to ensure that the vertebrae were in contact through these joints. Later, through Boolean operations, surface contact between the facets was guaranteed. Four-node tetrahedral elements were used with maximum 1.0 mm size for most of the elements of the structure. A refinement of 0.3 mm was applied to the elements from the joint contact region. A transition region was designed so that there was no abrupt variation in element size, which could create numerous deformed elements. In this region, 0.5 mm elements were used.

Mesh sensitivity tests were performed and four distortion measures were taken: aspect ratio, Jacobian, tetra collapse and volumetric skew. Thoracic models presented the following results: aspect ratio (admissible value < 5.0), 724 elements failed in the kyphosis model and 298 failed in the model with absence of kyphosis, which is equivalent to 0.01 and 0.00% of all elements of the model; Jacobian (admissible value > 0.5), no element failing the models with and without kyphosis, which equals 0.00% of all elements of the model; tetra collapse (admissible value > 0.1), 113 elements failed in the kyphosis model and 55 failed in the model with absence of kyphosis, which corresponds to 0.00% of all elements of the model; volumetric skew (admissible value < 0.7); 23,248 failed in the kyphosis model and 87,261 failed in the model with absence of kyphosis, which is equivalent to 0.35 and 1.30%, respectively, of all elements of the models. The final FE model included 6,698,616 elements with 1,248,982 nodes. HyperView (v14.0, Altai) was used for post-processing. The hardware used in this study was the HP Z820 Workstation with an Intel Xeon E5-2620 2.00 GHz processor with 64 GB of RAM and an NVIDIA video card (model QUADRO K2000D).

3.2 Materials properties

Despite the linear behavior attributed to the materials, confirmed by the low stress levels obtained in the results, the geometric nonlinearity was considered for the study of column stability. The vertebral material, mainly bone, was considered linear and isotropic. To reduce the computational cost, an entire vertebra was assumed to be a homogeneous body in a cortico-cancellous medium, combining both tissues. For analysis displacements, as in the present

Table 1 Vertebrae dimensions (mm)

Vertebra	WTP	DUP	DLP	HVB	DP	HP	LSP	WP
T5	48.88	19.44	20.64	11.50	1.44	8.96	41.68	24.57
T6	49.04	20.80	21.52	12.35	1.60	9.60	43.04	25.66
T7	48.32	21.92	22.8	12.92	1.36	9.44	40.40	26.48
T8	47.92	22.32	23.52	13.28	1.52	10.00	42.24	27.76
T9	47.44	23.44	24.80	13.70	1.44	11.12	41.04	30.03
T10	46.72	24.40	25.28	14.34	1.44	11.76	39.44	32.21
Adolescent/adult	80%	80%	80%	71%	80%	80%	80%	91%

WTP width of transverse process, DUP depth of upper plateau, DLP depth of lower plateau, HVB height of vertebral body, DP depth of pedicle, HP height of pedicle, LSP length of spinous process, WP width of plateau
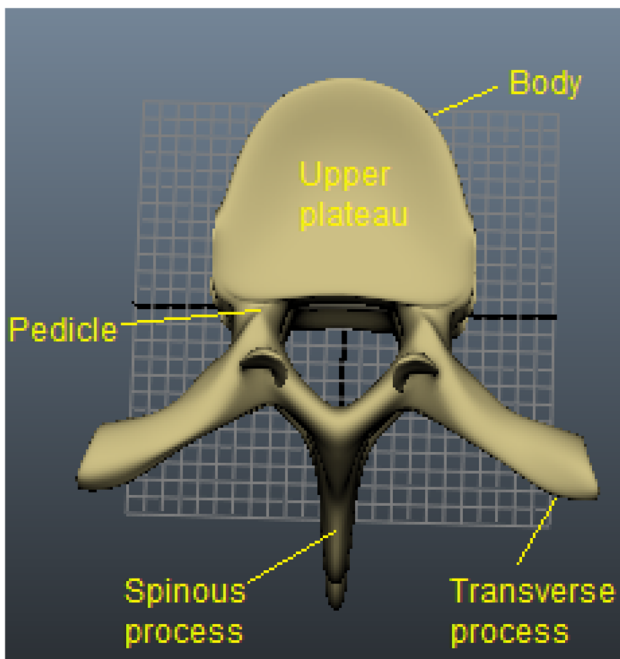
Fig. 2 Vertebra main components

study, this simplification is supported by previous studies on the calculation of an apparent elastic modulus of a cortico-cancellous medium of thoracic and lumbar vertebrae [8]. These values are closer to the characteristics of cancellous bone than to cortical bone.

To obtain a differential equation suitable for geometrical nonlinear analysis, but considering elastic behavior, one can start from the equilibrium equation of stress components.

$$\sigma_{ji,j} + B_i = 0, \tag{1}$$

where $i = 1, 2, 3$ (free index) and $j = 1, 2, 3$ (dummy index). σ_{ji} represents the symmetrical stress tensor and B_i represents the vector of body forces.

The considered strain–displacement differential equation is based on the engineering strain measure [11], considering the same indexes variation. ε_{ij} represents the symmetrical strain tensor and u_i (or u_j) the nodal displacement vector.

$$\varepsilon_{ij} = \frac{1}{2}(u_{i,j} + u_{j,i}). \tag{2}$$

The elastic constitutive equation is given by:

$$\sigma_{ij} = C_{ijkl}\varepsilon_{kl}, \tag{3}$$

where $i, j = 1, 2, 3$ (free index) and $k, l = 1, 2, 3$ (dummy index). The fourth-order tensor C_{ijkl} is the constitutive tensor.

Combining Eqs. (1–3), it is possible to obtain the classical Navier equation expressed in terms of displacements, strains and body forces [15].

$$\mu u_{i,kk} + (\lambda + \mu)\varepsilon_{kk,i} + B_i = 0, \tag{4}$$

or the system of equations can also be expressed in terms of displacements and body forces, as follows:

$$\mu u_{i,kk} + (\lambda + \mu)u_{k,ki} + B_i = 0, \tag{5}$$

where $i = 1, 2, 3$ (free index) and $k = 1, 2, 3$ (dummy index).

The constants of Lamé as given by:

$$\mu = \frac{E}{2(1 + v)}, \tag{6}$$

$$\lambda = \frac{Ev}{(1 + v)(1 - 2v)}. \tag{7}$$

Considering the complex behavior of some biomechanical materials, that can include viscoelastic and hyperelastic behaviors, the simulations based on Navier equation are feasible for large global displacements and rotations evaluation, but not for large strains.

In the present study, an equivalence calculation was performed through a computer simulation for two vertebrae, one using cortical and trabecular bone properties and

the other without differentiating between the two types of bone, to find the modulus of elasticity of the cortico-cancellous model. A load was applied and the modulus of longitidunal elasticity (E) that resulted in the same deformation in both models was calculated. A value of 948 MPa was found for the modulus of elasticity cortico-cancellous bone [7]. For the intervertebral discs, the modulus of elasticity values of 454 and 4 MPa were used for the annulus matrix and nucleus pulposus, respectively [9]. A Poisson coefficient (v) of 0.3 was applied to the bone component, 0.3 and 0.499 to the annulus matrix and nucleus pulposus, respectively. These values for the Poisson coeficients were obtained for the works of Kurutz [19], Schmidt et al. [33], Rohlmann et al. [30], Zander et al. [43], Lu et al. [22].

The flavum, intertransverse, and supraspinous ligaments used in the study were considered one-dimensional GAP type elements. A rope configuration was used to provide an option to exercise traction alone and their cross-sectional areas obtained from literature data [38].

$$k = \frac{EA}{L_0}, \tag{8}$$

where k represents the ligament stiffness constant and L_0 represents the initial length of the ligament.

The stiffness constant of the model's three ligaments was calculated, which resulted in 55 values of (k) for each model. An initial deformation of 0.5% was applied to all ligaments according to the literature [38]. Therefore, the pre-tensile values applied to the flavum, intertransverse, and supraspinous ligaments were 0.375, 0.09, and 0.65 N, respectively. A 10 N force was applied to the flavum and intertransverse ligaments on the right side, on the T8–T9 segment, whose value was based on the studies of Stokes and Gardner-Morse [36]. An asymmetric load was not applied to the supraspinous ligament, as it was only included in the model to ensure the connection between the spinous processes. The vertebrae and disks were considered as 4-node tetrahedral 3D elements.

3.3 Initial and boundary conditions

Rigid contact between the disks and the vertebrae, and sliding contact between facets was assumed. The interaction between the ring and the disk nucleus was represented as a nodal compatibility. In the upright position, the gravitational forces attributed to body weight are the primary loads supported by the spine. The load in a given mobile segment of the human spine may be considerably greater than the corresponding portion of body weight. The contraction of strong muscles, apply a high compressive force to it and, together with the abdominal musculature,

contribute to vertebral stabilization when in the orthostatic position [19]. Thus, an axial force (y axis) of 400 N was applied as pressure over a circular region on the upper face of the body of T5, at 1.30 N/mm^2. This value is valid for an adolescent weighing, approximately, 43 kg [9]. In addition, an unbalance load of 10 N was applied on the ligament, between functional unit T8–T9, as shown at the right side of Fig. 3. Total restriction, in the form of crimping, was applied to the lower face of T10 (Fig. 3).

The solution of the simulation was done for three sequential time-steps with a non-linear quasi-static type analysis. This configuration was employed because it is expected that there is a complex movement between the facet joints, with asymmetrical sliding and possibly high intensities. Each time-step used 10 increments and a maximum of 50 iterations to achieve convergence. The first time-step aimed at the detection and activation of the contacts between the articular facets without applying any load, activating the non-linear contact, in which it allowed the sliding without the joint separation in the subsequent time-steps. The second time-step aimed at including unbalance of ligament efforts (comparable to the lying down). In the last step, the body weight was included on the top of the T5 vertebra, thus representing the standing position with the unbalance of the ligament efforts. At all stages, the lower face of the T10 vertebra was completely fixed.
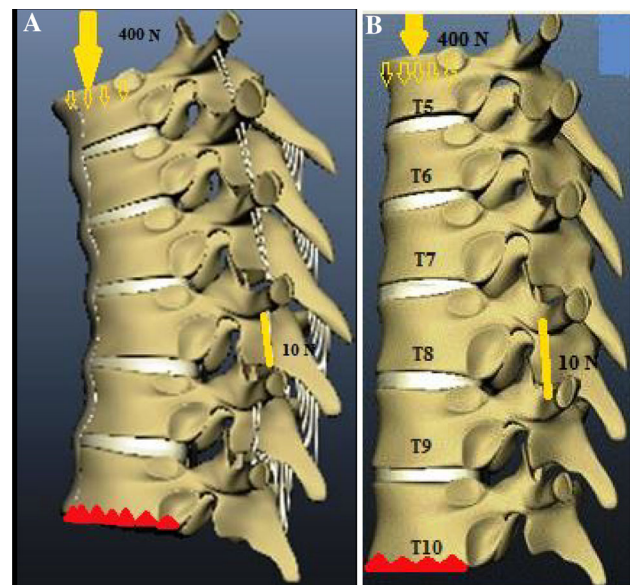
Fig. 3 T5–T10 segment in volumetric mesh for two conditions **a** kyphosis, with representation of the axial load of 400 N and an unbalance load of 10 N applied on the ligament, at the right, between functional unit T8–T9; **b** the absence of kyphosis and same initial/boundary conditions

4 Results

4.1 Rotational displacement

The greatest rotational displacement of the T8–T9 functional unit was observed in the case of absence of kyphosis. Moreover, in the absence of an axial load and applying the asymmetric ligament load alone, the rotations were even greater. The displacements (mm) of the T8–T9 mobile segment are shown in Fig. 4a and b in the case of kyphosis and the absence of kyphosis, respectively, with an asymmetric load on the right flavum and intertransverse ligaments. In the case of absence of kyphosis (B), a misalignment of the vertebrae's central axis was observed, due to a displacement in X axis of the spinous processes of both vertebrae, 0.115 mm in T8, and − 0.653 mm in T9, as well as the approximation of the transverse processes of T8 and T9, characterizing a lateral flexion of the vertebrae to the right. A smaller displacement was observed in the case of kyphosis (A).

The deviations were also measured according to the Cobb angle for scoliosis. This angle is that between the upper plateau of the vertebra superiorly located to the deviation and the lower plateau of the vertebra inferiorly located to the deviation. The Cobb angles, in the presence of asymmetry ligaments load, in the segments with preserved kyphosis and absence of Kyphosis, is represented in Fig. 5.

Figure 6 shows the rotational displacement in [mm], in top view of the T9 vertebra, where a near zero displacement is observed in the preserved kyphosis condition (A), and a greater T9 displacement in the absence of kyphosis condition (B).

Axial rotational displacement, in degrees, of vertebrae T8 and T9, are shown in the Table 2.

4.2 Shear stresses

The maximum shear stresses in the facets in the case of kyphosis, an asymmetric ligament load, and axial pressure were higher than in the case of absence of kyphosis. Values between 5 and 12.5 MPa were observed in the upper facets of T9; whereas the lower facets yielded values between 2.5 and 7.5 MPa. In the case of absence of kyphosis under the same loading conditions, values of 7.5 MPa were observed in the upper facets of T9 and values close to zero were observed in the lower ones.

4.3 Compressive stresses in the intervertebral disks

In the case of kyphosis, with an asymmetric load on the flavum and intertransverse ligaments, as well as an axial load, greater compressive stresses were observed in the anterior portion of all disks, with values ranging from −2.86 to − 0.64 MPa. In the case of absence of kyphosis, the compressive stresses were close to zero.
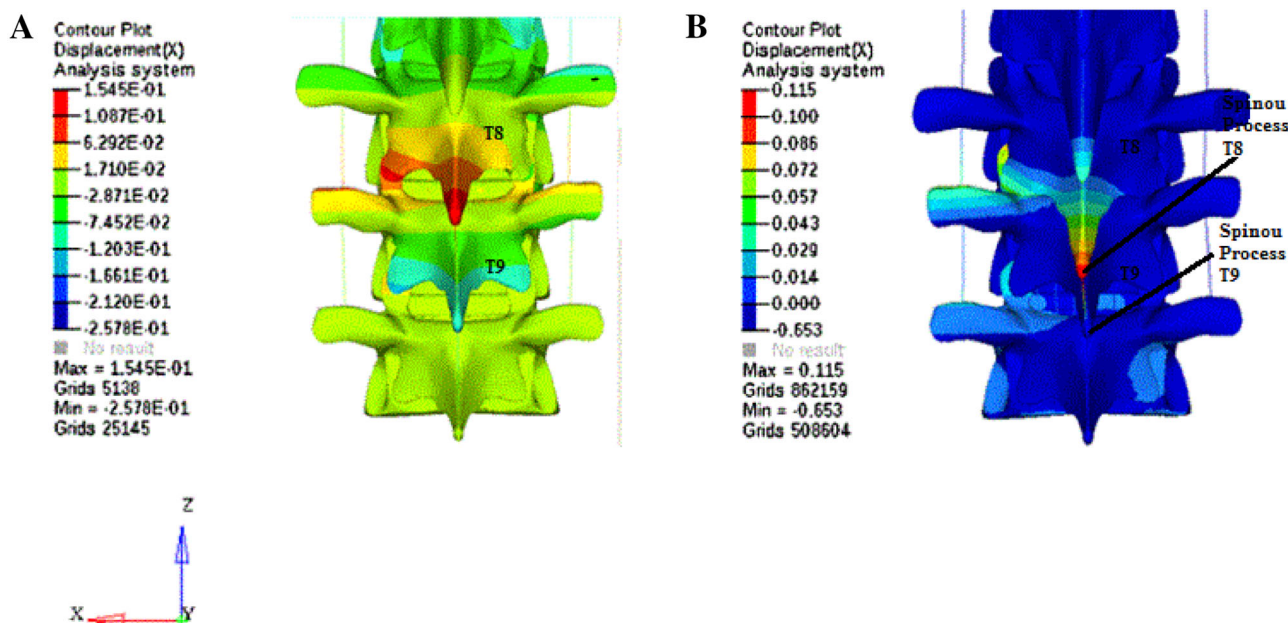

Fig. 4 a Displacements (mm) of the T8–T9 functional unit, in kyphosis, and force unbalance in the flavum and intertransverse ligaments; b displacements (mm) of the T8–T9 functional unit, in the absence of kyphosis, and unbalance in the flavum and intertransverse ligaments

Fig. 5 Cobb angle measurement of T8–T9 segments, under asymmetric loading conditions on flavum and intertransverse ligaments, **a** thoracic segment in kyphosis, zero degrees; **b** thoracic segment in absence of kyphosis, Cobb of 2.85°
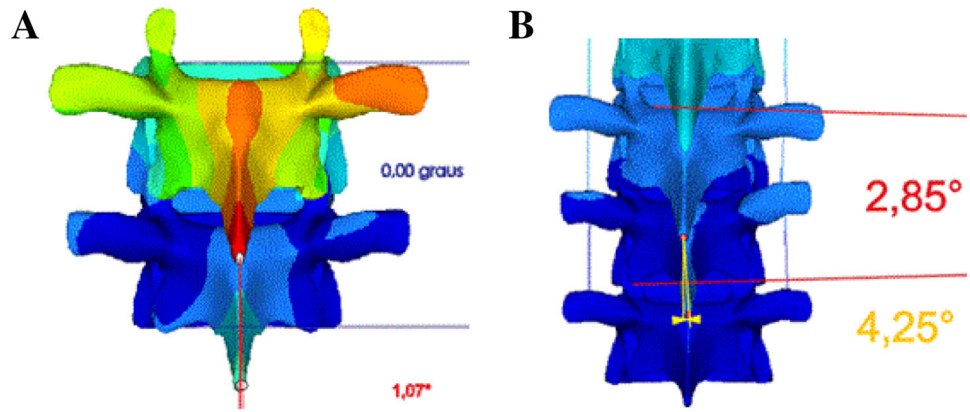
Fig. 6 a Displacements (mm) of the T9 vertebra, in top view, kyphosis condition, and force unbalance in the flavum and intertransverse ligaments; **b** displacements (mm) of the T9, in the absence of kyphosis, and unbalance in the flavum and intertransverse ligaments
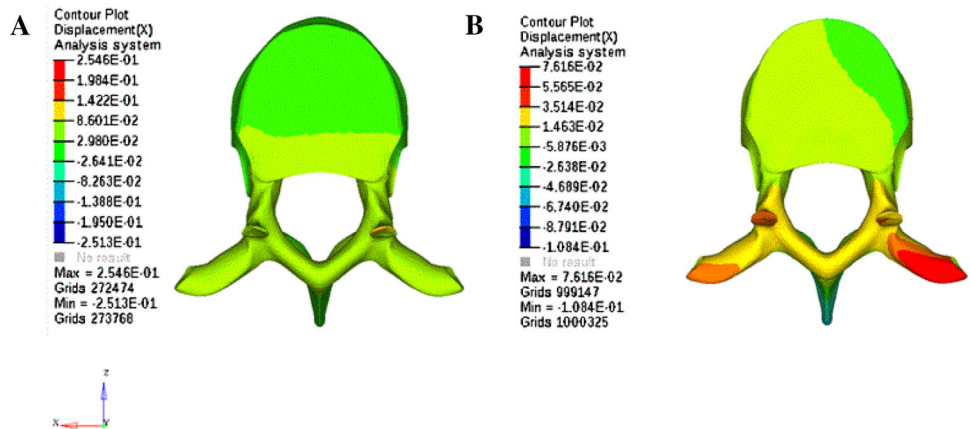
Table 2 Axial rotational displacement of the vertebrae T8 and T9, in kyphosis and the absence of kyphosis, under axial load (400 N) and asymmetric ligament load (10 N) and, only, asymmetric ligament load (10 N)

Loads (N)	Rotational displacement T8 and T9 (°)	
	Kyphosis	Absence of kyphosis
Asymmetric ligament load	T8 0.11 (clockwise)	T8 0.16 (clockwise)
	T9 0.02 (counter-clockwise)	T9 0.06 (counter-clockwise)
Asymmetric ligament load	T8 0.12 (clockwise)	T8 0.22 (clockwise)
	T9 0.05 (counter-clockwise)	T9 0.08 (counter-clockwise)

5 Discussion

The considered model was defined to analyze the displacements and rotations of the vertebral body and facet joints in kyphosis and hypokyphosis conditions, under physiological loading. It was verified that in the condition of hypokyphosis, the column is more unstable to the vertebral rotations, when compared to the condition of kyphosis, corroborating previous studies of Castelein et al. [3] and Kouwenhoven et al. [17]. The considered models used in this kind of analyses are sensitive to the action of loads on the spine structures. This fact may have important clinical implications, such as the association of the spine morphology of children and adolescents and the risk of

vertebral deformation and spinal damage. The results obtained in the present study, in association with previous studies, allow to infer conclusions that can change paradigms in the adolescent spine assessment.

A 3D modeling technique of the human anatomy was tested from graphical images for use in numerical computational analysis with FEM. The results obtained in this study reveal a versatile methodology able to vary the parameters of the structures described, such as using data from the 10-year-old girl spine geometry obtained from Meijer [23] studies, or vary the morphology of a particular structure. Moreover, it exhibits good graphic quality and allows visualization of models in different perspectives. Other models for different populations and age groups, and

different morphologies should be proposed. The use of three images, in three planes, increased the quality of the final model generated by graphical images. Further studies are needed to improve alternative geometric modeling methods to MRI and CT, especially for application in non-patient-specific finite element model studies.

The present study is important to draw attention and stimulate further studies with theoretical spine models of individuals without complete bone maturation. It is unprecedented in the generation of the anatomical geometric model, as well as in the simulation of the same vertebral segment in two different morphological conditions. However, there are limitations in the model presented. The scarcity of data on the material properties of the biological tissues of young individuals and the absence of soft tissue structures in the model presented, such as muscles, joint capsules and other ligaments, somehow deplete the quantitative analysis of displacements. In a joint, only the passive stiffness of its structure is not sufficient to maintain stability in daily tasks.

A biomechanical study of the T5–T10 thoracic segment of an adolescent was conducted to compare the biomechanical effects on the stability of the vertebrae when its curvature is altered in the sagittal profiles, in the presence of axial load and asymmetric ligament load. The T5–T10 segment is important for its vulnerability to spinal deformity in young people. Experimental studies have reported the importance of this thoracic segment in the initialization and progression of the spinal deformity adolescent idiopathic scoliosis (AIS) [3, 17].

There is no precedent in the literature regarding the generation of geometric models based on graphs for use in FEM simulations. A geometric model of the thoracic spine was created with proper orientation of the joint facets and geometric adolescent vertebrae data. Smaller and more complex anatomical structures, such as the facet joints and cortical shell, are below the resolution of techniques such as biplane or CT imaging and cannot be indicated in vivo due to high doses of radiation [8]. A possible vantage in the use of computer graphics and digitization software, from graphic images, is the geometric control provided by the program, including solving contact problems, or reducing excessive detail before exporting the .stl mesh. The present model is a close representation of the actual model when compared to those depicting cylinders and bars [10], typical volumetric models with a single mobile segment [24] or volumetric models that omit the back portion of the vertebrae [9].

The low stress levels obtained for physiological loads justify the linear constitutive models adopted for the materials. In this respect, the model developed will enable a good quantitative assessment of displacement and rotation in the system, but may exhibit differences in stress and strain levels. An accurate model to evaluate stress and strain should consider the imperfections, porous, viscous and elastoplastic behavior of the material, considered complex parameters for accurate modeling. Additionally, the computational costs of complex models should also be taken into account. The viscoelastic properties of the intervertebral disk were not taken into account, since experimental data for model calibration are not available. In addition, the viscoelastic parameters are not constant and depend on the state of stresses resulting from the requests. The choice of the constants, mentioned above, for disc representation was based on the literature and justified by the difficulty, or impossibility, of obtaining parameters related to constitutive models for the rubber that can be used in the models available in the literature, such as Arruda-Boyce, Neo-Hookean, Yeoh, Mooney-Rivlin, Ogden [1].

A FEM study need to be constructed based on age-specific biomechanical data. In a review study, Wang et al. [40] reported that all the models surveyed used material and biomechanical data derived from adults. According to the authors, there is little biomechanical information concerning young vertebral columns owing to the difficulty in obtaining anatomical parts of the human spine from fresh cadavers. This issue was a challenge for this study. There are few studies that present the modulus of elasticity for the vertebrae tissues of younger individuals and the available values vary considerably.

Another challenge is the anatomical complexity of the human thorax, where the thoracic spine is located. It is known that the vertebral thoracic segment is encased in a closed system composed of bones from the rib cage, internal thoracic organs, and a complex system of fascias and muscles, the action of which increases the critical load and, consequently, vertebral stability. However, the complexity of the structure and the diversity in the orientation of muscular actions make it difficult to include in the study. Few computational models include the ribs and posterior elements of the spine [21, 2]. According to Van Der Plaats et al. [38], improving the model by incorporating the ribs and muscles is a major challenge to be overcome. However, the comparison between two different profiles of the same model allows to reach relevant conclusions concerning the structural behavior of the adolescent thoracic segment.

In an FE simulation using the geometric model proposed here, tetrahedral linear elements were used due to software limitations in generating the mesh of quadratic elements. To compensate for this limitation, we opted to control the mesh by increasing the density of elements in regions where more complex behavioral stress are assumed. It is important to underscore that the finite element method is a

mathematical approximation, making it necessary to consider the gains and losses of different equation choices.

In present study, the assessment of the rotational stability of vertebra under kyphosis of 31.24°, under absence of kyphosis and ligament imbalance, was performed. It was observed that the vertebra below the imbalance (T9) showed displacement levels similar to the obtained from deformity of scoliosis. This result is in agreement with the study of Van Der Plaats et al. [38], that present an axial rotation of the vertebral bodies towards the convexity of the lateral curve. The study demonstrated that the rotation of T8 in relation to T9 was greater in the case of absence of kyphosis and in the absence of an axial load. These findings corroborate the hypothesis of Castelein et al. [3], in which the authors describe a greater demand on the facet joints associated with greater efficiency in the containment of the rotation of a vertebra in relation to the adjacent vertebra. In an experimental study, Panjabi et al. [27] evaluated the coefficients of stiffness and flexibility in the thoracic spine segments. The authors concluded that a thoracic functional unit is more flexible in traction than in compression. This could justify the greater rotational displacement of the T9 vertebra in this study when the axial load was removed. These findings contribute to the search for preventive actions of adolescent idiopathic scoliosis. The models analyzed in the study were sensitive to the action of loads on the spinal structures. This may have important clinical implications, such as the association of the spinal morphology of children and adolescents and the risk of vertebral deformation and spinal damage. Considering the complexity of biological structures and risks involving in vivo studies, the continuous improvement of computational modeling techniques using FEM is relevant.

6 Conclusion

The applicability test of 3D geometric modeling of the T5–T10 thoracic segment, with the simplifications controlled, using graphical references and anatomical measurements of the literature and later applied in a numerical computational analysis with FEM, was satisfactory and has potential for other qualitative biomechanical studies. However, the stress and strain analyses need to be better evaluated in future studies. The developed model allowed a good quantitative evaluation of the displacement and rotation in the system. It was found that the facet joints were less requested, and there were more pronounced vertebral rotations in the vertebral segments subject to imbalance of ligamentous forces, in the adolescent thoracic spine in the absence of kyphosis. These findings contribute to the search for preventive actions of adolescent idiopathic scoliosis.

For future studies, the model generated in the present study may serve to study the optimal functional kyphosis angle for the adolescent thoracic spine and for analysis of asymmetric equilibrium of deep plane musculature of the thoracic spine, such as the intertransversal, interspinal and transverse-spinal.

References

1. Ali A, Hosseini M, Sahari BB (2010) A review and comparison on some rubber elasticity models. J Sci Ind Res 69:495–500
2. Cahill PJ, Wang W, Asghar J, Booker R, Betz RR, Ramsey C, Baran G (2012) The use of a transition rod may prevent proximal junctional kyphosis in the thoracic spine following scoliosis surgery: a finite element analysis. Spine 37(12):E687–E695
3. Castelein RM, Van Dieen JH, Smit TH (2005) The role of dorsal shear forces in the pathogenesis of adolescent idiopathic scoliosis—a hypothesis. Med Hypotheses 65:501–508
4. Cheng FH, Shih SL, Chou WK, Liu CL, Sung WH, Chen CS (2010) Finite element analysis of the scoliosis spine under different loading conditions. Bio-Med Mater Eng 20(5):251–259
5. Clément JL, Geoffray A, Yagoubi F, Edouard C, Solla F, Oborocianu I, Rampal V (2013) Relationship between thoracic hypokyphosis, lumbar lordosis and sagittal pelvic parameters in adolescent idiopathic scoliosis. Eur Spine J 22:2414–2420
6. Dickson RA, Lawton JO, Archer IA, Butt WP (1984) The pathogenesis of idiopathic scoliosis: biplanar spinal asymmetry. J Bone Joint Surg 66(1):8–15
7. Dong L, Li G, Mao H, Marek S, Yang KH (2013) Development and validation of a 10-year-old child ligamentous cervical spine finite element model. Ann Biomed Eng 41(12):2538–2552
8. El Masri F, Sapin de Brosses E, Rhissassi K, Skalli W, Mitton D (2012) Apparent young's modulus of vertebral cortico-cancellous bone specimens. Comput Methods Biomech Biomed Eng 15(1):23–28
9. Fok J, Adeeb S, Carey J (2010) FEM simulation of non-progressive growth from asymmetric loading and vicious cycle theory: scoliosis study proof of concept. Open Biomed Eng J 4:162–169
10. Ghista DN, Vivian GR, Subbaraj K, Lozada PJ, Srinivasan TM, Barnes G (1988) Biomechanical basis of optimal scoliosis surgical-correction. J Biomech 21(2):77–88
11. Greco M, Rocha da Costa LJ (2012) Discussion on The logarithmic strain measure applied to the nonlinear positional formulation for space truss analysis [Finite Element in Analysis and Design 45 (2009) 632 639] and Nonlinear positional formulation for space truss analysis [Finite Element in Analysis and Design 42 (2006) 1079 1086]. Finite Elem Anal Des 52(1):93–95
12. Janssen MM, Drevelle X, Humbert L, Skalli W, Castelein RM (2009) Differences in male and female spino-pelvic alignment in asymptomatic young adults: a three-dimensional analysis using upright low-dose digital biplanar X-rays. Spine 34(23):E826–E832

13. Janssen MM, Vincken KL, Kemp B, Obradov M, De Kleuver M, Viergever MA et al (2010) Pre-existent vertebral rotation in the human spine is influenced by body position. Stud Health Technol Inform 19:1728–1734

14. Jaramillo HE, Gomez L, Garcia JJ (2015) A finite element model of the L4-L5-S1 human spine segment including the heterogeneity and anisotropy of the discs. Acta Bioeng Biomech 17(2):15–24

15. Karasudhi P (1991) Foundations of solid mechanics, 1st edn. Kluwer, Waterloo, pp 98–102

16. Kotwicki T (2008) Intravertebral deformation in idiopathic scoliosis—a transverse plane computer tomographic study. J Pediatr Orthop 28:225–229

17. Kouwenhoven JWM, Smit TH, Van Der Veen AJ, Kingma I, Castelein RM (2007) Effects of dorsal versus ventral shear loads on the rotational stability of the thoracic spine. Spine 32:2545–2550

18. Kuo CS, Hu HT, Lin RM, Huang KY, Lin PC, Zhong ZC et al (2010) Biomechanical analysis of the lumbar spine on facet joint force and intradiscal pressure: a finite element study. BMC Musculoskelet Disord 11:151–164

19. Kurutz M (2010) Finite element modelling of human lumbar spine. In: Moratal D (ed) Finite element analysis. InTech, pp 209–236. ISBN: 978-953-307-123-7

20. Lan CC, Kuo CS, Chen CH, Hu HT (2013) Finite element analysis of biomechanical behavior of whole thoracic-lumbar spine with ligamentous effect. Changhua J Med 11:26–41

21. Little JP, Adam C (2011) Patient-specific computational biomechanics for simulating adolescent scoliosis surgery: predicted vs clinical correction for a preliminary series of six patients. Int J Numer Methods Biomed Eng 27:347–356

22. Lu YM, Hutton WC, Gharpuray VM (1996) Can variation in Intervertebral disc height affect the mechanical function of the disc? Spine 21:2208–2217

23. Meijer GJM (2011) Development of a non-fusion scoliosis correction device numerical modelling of scoliosis correction, Ph.D. Thesis—College voor Promoties, Universiteit Twente, 165f. Enschede, The Netherlands

24. Meijer GJM, Homminga J, Hekman EEG, Veldhuizen AG, Verkerke GJ (2010) The effect of three-dimensional geometrical changes during adolescent growth on the biomechanics of a spinal motion segment. J Biomech 43(8):1590–1597

25. Nault ML, Thiong JMM, Roy-Beaudry M, Turgeon I, De Guise J, Labelle H et al (2014) Three-dimensional spinal morphology can differentiate between progressive an nonprogressive patients with adolescent idiopathic scoliosis at the initial presentation. Spine Deformity 39(10):E601–E606

26. Pal GP (1991) Mechanism of production of scoliosis: a hypothesis. Spine 16:288–292

27. Panjabi MM, Brand RA, White AA (1976) Mechanical properties of the human thoracic spine. J Bone Joint Surg 58-A:642–652

28. Panjabi MM, Takata K, Goel V (1991) Thoracic human vertebrae-quantitative three-dimensional anatomy. Spine 16:889–901

29. Ran B, Zhang GY, Shen F, Chen JY, Wu JB, Zhao FC et al (2014) Comparison of the sagittal profiles among thoracic idiopathic scoliosis patients with different Cobb angles and growth potentials. J Orthop Surg Res 9:19

30. Rohlmann A, Zander T, Bergmann G (2006) Spinal loads after osteoporotic vertebral fractures treated by vertebroplasty or kyphoplasty. Eur Spine J 15:1255–1264

31. Roussouly P, Labelle H, Rouissi J, Bodin A (2013) Pre- and postoperative sagittal balance in idiopathic scoliosis: a comparison over the ages of two cohorts of 132 adolescents and 52 adults. Eur Spine J 22(2):S203–S215

32. Schlosser TP, Shah SA, Reichard SJ, Roger K, Vincken KL, Castelein RM (2014) Differences in early sagittal plane alignment between thoracic and lumbar adolescent idiopathic scoliosis. Spine J 2(14):282–290

33. Schmidt H, Heuer F, Wilke HJ (2009) Which axial and bending stiffnesses of posterior implants are required to design a flexible lumbar stabilization system? J Biomech 42:48–54

34. Sevastik J, Aaro S, Normelli H (1984) Scoliosis: experimental and clinical studies. Clin Orthop Relat Res 191:27–34

35. Stokes IAF, Burwell RG, Dangerfield PH (2006) Biomechanical spinal growth modulation and progressive adolescent scoliosis: a test of the "vicious cycle" pathogenetic hypothesis: summary of an electronic focus group debate of the IBSE. Scoliosis 1:16

36. Stokes IA, Gardner-Morse M (1991) Analysis of the interaction between vertebral lateral deviation and axial rotation in scoliosis. J Biomech 24(8):753–759

37. Tyndyk MA, Barron V, Mchugh PE, O'Mahoney D (2007) Generation of a finite element model of the thoracolumbar spine. Acta Bioeng Biomech 9:35–46

38. Van Der Plaats A, Veldhuizen AG, Verkerke GJ (2007) Numerical simulation of asymmetrically altered growth as initiation mechanism of scoliosis. Ann Biomed Eng 35:1206–1215

39. Villemure I, Aubin CE, Dansereau J, Labelle H (2002) Simulation of progressive deformities in adolescent idiopathic scoliosis using a biomechanical model integrating vertebral growth modulation. J Biomech Eng 124:784–790

40. Wang W, Baran GR, Betz RR, Samdani AF, Pahys JM, Cahill PJ (2014) The use of finite element models to assist understanding and treatment for scoliosis: a review paper. Spine Deformity 2:10–27

41. White AA (1971) Kinematics of the normal spine as related to scoliosis. J Biomech 4:405–411

42. Willner S, Johnson B (1983) Thoracic kyphosis and lumbar lordosis during the growth period in children. Acta Paediatr Scand 72(6):873–878

43. Zander T, Rohlmann A, Calisse J, Bergmann G (2001) Estimation of muscle forces in the lumbar spine during upper body inclination. Clin Biomech 16:73–80